Prediction of a Novel Magnetoelectric Switching Mechanism in Multiferroics

Yurong Yang,[1,2] Jorge Íñiguez,[3] Ai-Jie Mao,[4] and L. Bellaiche[1]

[1]*Physics Department and Institute for Nanoscience and Engineering, University of Arkansas, Fayetteville, Arkansas 72701, USA*
[2]*Physics Department, Nanjing University of Aeronautics and Astronautics, Nanjing 210016, China*
[3]*Institut de Ciència de Materials de Barcelona (ICMAB-CSIC), Campus UAB, 08193 Bellaterra, Spain*
[4]*Institute of Atomic and Molecular Physics, Sichuan University, Chengdu 610065, China*
(Received 30 May 2013; published 5 February 2014)

We report a first-principles study of the recently predicted $Pmc2_1$ phase of the multiferroic $BiFeO_3$ material, revealing a novel magnetoelectric effect that makes it possible to control magnetism with an electric field. The effect can be viewed as a two-step process: Switching the polarization first results in the change of the sense of the rotation of the oxygen octahedra, which in turn induces the switching of the secondary magnetic order parameter. The first step is governed by an original trilinear-coupling energy between polarization, octahedral tilting, and an antiferroelectric distortion. The second step is controlled by another trilinear coupling, this one involving the predominant and secondary magnetic orders as well as the oxygen octahedral tilting. In contrast with other trilinear-coupling effects in the literature, the present ones occur in a simple ABO_3 perovskite and involve a large polarization.

Multiferroics have experienced a resurgence of interest because of their inherent cross coupling between electric and magnetic degrees of freedom [1–7]. In particular, a systematic control of the magnitude and crystallographic direction of magnetic order parameters by an electric field is attractive for the design of original devices, and fundamentally interesting. One way to attain such control is via the existence of an energy term ΔE that (1) directly couples magnetic moments and electric polarization $\mathbf{P}$ and (2) is linear in $\mathbf{P}$. Familiar examples of such an energy term are specific Dzyaloshinskii-Moriya interactions [8–10] of the form $\Delta E \sim \mathbf{P} \cdot (\mathbf{L} \times \mathbf{M})$ [10,11], the Lifshitz invariants $\Delta E \sim \mathbf{P} \cdot [\mathbf{L}(\nabla \cdot \mathbf{L}) + \mathbf{L} \times (\nabla \times \mathbf{L})]$ and $\Delta E \sim \mathbf{P} \cdot [\mathbf{M}(\nabla \cdot \mathbf{M}) - (\mathbf{M} \cdot \nabla)\mathbf{M})]$ [12,13], where $\mathbf{L}$ and $\mathbf{M}$ are the antiferromagnetic vector and magnetization, respectively. Another example is the spin-current model [14–16] for which $\Delta E \sim (\mathbf{P} \times \mathbf{e}_{ij}) \cdot (\mathbf{m}_i \times \mathbf{m}_j)$, where $\mathbf{e}_{ij}$ is the unit vector joining site i to site j and where $\mathbf{m}_i$ and $\mathbf{m}_j$ are the magnetic moments located at these sites i and j.

The pioneering work of Ref. [17] also shows that there is another way to control magnetic quantities by electric polarization. This can be thought of as indirect since it consists of two steps. A trilinear "structural-only" coupling between polarization and two different oxygen octahedral tilting modes (also termed antiferrodistortive or AFD motion) first leads to the reversal of one octahedral tilt when switching the polarization. Then, this reversal can result in the change of direction of a magnetic order parameter (via a second energy that was not provided in Ref. [17] and that should couple magnetic moments and octahedral tilt). It is important to know if other two-step processes, allowing a systematic control of magnetic properties by electrical polarization, can exist. In particular, can the first energy also involve another kind of structural quantity, in addition to

polarization and AFD motions, namely, antiferroelectricity? Another question to resolve is to determine the expression of the second energy that couples magnetic degrees and the polarization-switchable structural property.

We provide answers to these issues via first-principles calculations. A novel two-step magnetoelectric effect is discovered. Its first energy is an original term that trilinearly couples polarization, one AFD distortion, and one antiferroelectric mode. This structural-only energy results in the change of the sense of the rotation of the oxygen octahedra when polarization is reversed. The second energy is another coupling involving predominant and secondary magnetic order parameters, as well as the AFD mode. It forces the secondary magnetic order parameter to switch its direction, once oxygen octahedral tilting is reversed by the change of sign of the polarization. The designation of the phenomenon as having two steps is made to indicate that two different energies are involved, even if the switchings of the two physical properties resulting from the existence of these two energies can be simultaneous.

Density-functional calculations within the local spin density approximation are performed for $BiFeO_3$ (BFO) systems, using the Vienna *ab initio* simulation package (VASP) [18]. As in Refs. [19–21], we also include a Hubbard correction for Fe ions, adopting the self-consistent value of $U = 3.8$ eV [22,23] (note that this choice of U provided a good agreement between theory and experiment even for films under a large magnitude of strain; see, e.g., Ref. [24] and references therein). Spin-orbit and noncollinear magnetism are taken into account, and the projected augmented wave method and an energy cutoff of 500 eV are employed. We focus on the orthorhombic $Pmc2_1$ phase of (001) BFO films that has recently been found for large enough tensile strain [20] (note that this state has also been predicted in $BaMnO_3$, $EuTiO_3$, or $CaTiO_3$, and that increasing the temperature should lead to a

decrease of the critical strain at which this phase becomes the ground state). A 40-atom supercell is used to model it, along with a $3 \times 3 \times 3$ k-point mesh. Its lattice vectors are $\mathbf{a}_1 = 2a_{IP}\mathbf{x}$, $\mathbf{a}_2 = 2a_{IP}\mathbf{y}$, and $\mathbf{a}_3 = a_{IP}[\delta_1\mathbf{x} + \delta_2\mathbf{y} + (2 + \delta_3)\mathbf{z}]$. a_{IP} is the in-plane lattice constant. It is chosen here to be 4.135 Å, which leads to a tensile strain of about 6% in BFO (note that BFO films experiencing strains having a magnitude even larger than 6% have been experimentally grown [25]). $\mathbf{x}$, $\mathbf{y}$, and $\mathbf{z}$ are unit vectors along the [100], [010], and [001] pseudocubic directions, respectively. The δ_1, δ_2, and δ_3 variables and the atomic positions are relaxed to minimize the total energy.

As sketched in Fig. 1, this $Pmc2_1$ state is characterized by (1) a polarization ($\mathbf{P}$) lying along an in-plane $\langle 110 \rangle$ direction, (2) a Bi-driven antiferroelectric (AFE) vector ($\mathbf{A}$) that is associated with the M point of the cubic, five-atom first Brillouin zone and that is oriented along an in-plane $\langle 1\bar{1}0 \rangle$ direction that is perpendicular to the polarization, and (3) by an in-phase oxygen octahedral tilting (that is also associated with the M point of the first Brillouin zone) about the out-of-plane [001] direction. Such a tilting is represented by a pseudovector ω for which the magnitude provides the value of the tilting angle while its direction is either parallel or antiparallel to the out-of-plane direction—indicating if this tilting is counterclockwise versus clockwise, respectively. The superposition of $\mathbf{P}$ and $\mathbf{A}$ results in cations moving in a zigzag pattern [20], as shown in the top panels of Fig. 1. The polarization is calculated from the Bloch representation of the modern theory of polarization [26]. The strength of the antiferroelectricity vector is estimated by $A = (d_{Bi,A}/d_{Bi,P})P$, where $d_{Bi,A}$ represents the atomic motion of Bi ions (along $\langle 1\bar{1}0 \rangle$) associated with antiferroelectricity, while $d_{Bi,P}$ is the Bi displacement (along $\langle 110 \rangle$) associated with the polarization P.

Let us denote by $+P$ and $-P$ the cases in which $\mathbf{P}$ is parallel or antiparallel to the [110] direction, respectively. Similarly, once we choose a specific Bi site to define the origin of the AFE vector [27], $+A$ and $-A$ represent the AFE vectors along $[1\bar{1}0]$ and $[\bar{1}10]$, respectively. Finally, once we select an Fe site to define the origin of the AFD motion [27], $+\omega$ and $-\omega$ indicate that the oxygen octahedral tiltings (about a specific line joining Fe atoms along [001]) are counterclockwise and clockwise, respectively. When considering the eight cases resulting from the combination of the positive and negative signs of $\mathbf{P}$, $\mathbf{A}$, and ω, we found that the ground state of the $Pmc2_1$ state is fourfold degenerate; namely, the $(+P, +A, +\omega)$, $(+P, -A, -\omega)$, $(-P, -A, +\omega)$, and $(-P, +A, -\omega)$ all have the same energy, as well as identical magnitude for their $\mathbf{P}$, $\mathbf{A}$, and ω vectors. The other four states $(-P, +A, +\omega)$, $(-P, -A, -\omega)$, $(+P, -A, +\omega)$, and $(+P, +A, -\omega)$ are unstable and transform to one of the four stable equilibrium states during relaxation. These results suggest the existence of a very peculiar physical energy that couples $\mathbf{P}$, $\mathbf{A}$, and ω in a very precise manner. The Supplemental Material [28] provides the expression of this energy term:

$$\Delta E_1 = -C_1 P A \omega, \qquad (1)$$

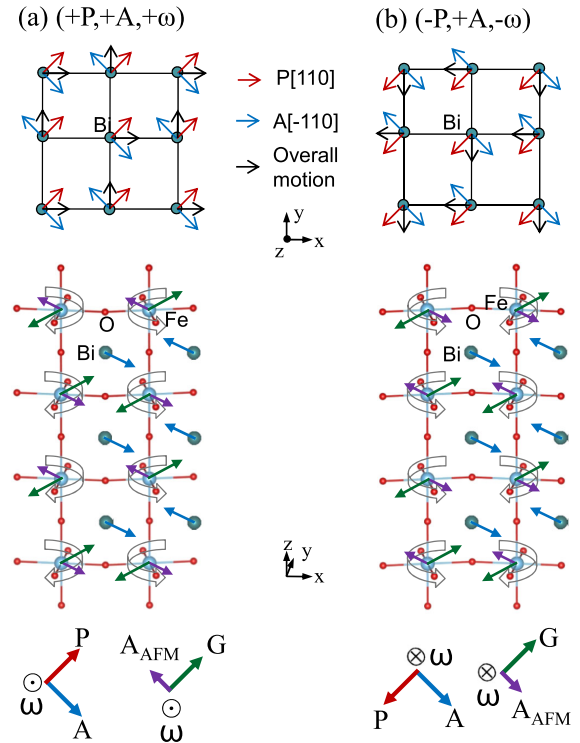where C_1 is a positive coupling parameter.

FIG. 1 (color online).   Schematization of properties in the equilibrium $(+P, +A, +\omega)$ state (left panels) and $(-P, +A, -\omega)$ phase (right panels). The upper panels display the zigzag motions of Bi atoms in an (x, y) plane. The middle panels show (i) oxygen octahedral tiltings (represented by curled arrows), (ii) magnetic dipoles associated with the weak A-type antiferromagnetic vector (purple arrows) and with the predominant G-type AFM vector (represented by green arrows), and (iii) Bi displacements that are associated with AFE (light blue arrows). The lettering "Fe" (respectively, "Bi") indicates the iron (respectively, bismuth) ion whose location serves as the origin for the definition of the ω, G, and A_{AFM} (respectively, A) vectors [27]. The lower panels schematize the directions of P, the AFE vector, the AFD vector, the G-type AFM vector, and the weak A-type AFM vector.

As characteristics of ferroelectrics, the application of an electric field that is opposed to an initial polarization direction should switch the polarization. According to Eq. (1), this switch should make the oxygen octahedra rotate from counterclockwise to clockwise, if the AFE vector maintains its direction. Equation (1) further suggests that reverting this electric field should then allow the oxygen octahedra to tilt again in a counterclockwise manner and thus hints towards a systematic control of the oxygen octahedral tilting direction by an electric field. To test such a possibility, Fig. 2(a) reports the total energy resulting from the variation of the polarization from its positive equilibrium value of $+1.12$ C/m^2 to its opposite, negative equilibrium value (along $[\bar{1}\,\bar{1}\,0]$), and vice versa. Figures 2(b) and 2(c) show the AFE vector and out-of-plane, in-phase octahedral tilting resulting from the atomic relaxation occurring for each considered value of the polarization selected during the pathways $(+P \rightarrow -P)$ and $(-P \rightarrow +P)$. They reveal that one can indeed go from the equilibrium $(+P, +A, +\omega)$ state to the equilibrium $(-P, +A,$
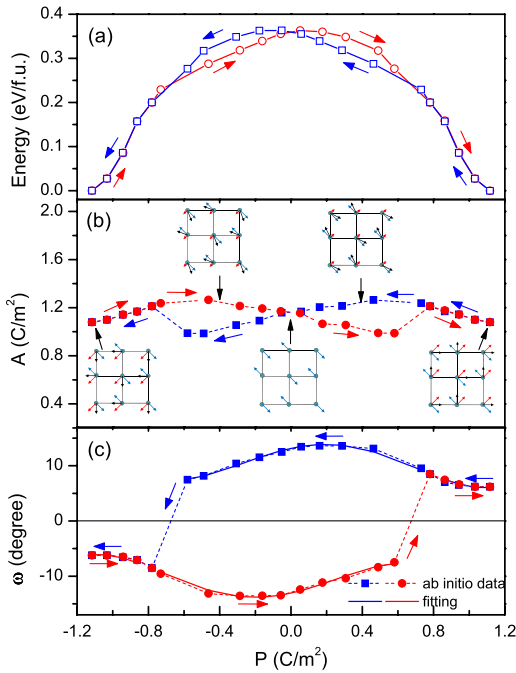
FIG. 2 (color online). Behavior of various quantities as a function of P, during the $(+P, +A, +\omega) \to (-P, +A, -\omega)$ and $(-P, +A, -\omega) \to (+P, +A, +\omega)$ pathways. (a),(b),(c) The total energy, AFE vector, and in-phase octahedral tilting, respectively. The insets of (b) schematize the evolution of the resulting Bi displacements along these paths, with the red, blue, and black arrows representing the polarization-induced, AFE-driven, and total Bi displacements, respectively. In (c), symbols represent data from first-principles calculations while the blue (respectively, red) solid line shows the fitting of these data by fourth order polynomials of P for positive (respectively, negative) ω.

$-\omega)$ phase (and vice versa) when continuously changing the magnitude and sign of the polarization. Such a transformation occurs via a pathway having an energy barrier of 0.36 eV per formula unit [29], along which the AFE vector does not vary too much. This implies, as shown in the insets of Fig. 2(b), that the overall cation displacement gradually evolves from a zigzag pattern (when A and P are close to each other in magnitude, that is, for a large magnitude of P) to a pure AFE pattern (which occurs when P vanishes). The overall symmetry of the structure always remains $Pmc2_1$ during the whole pathway, i.e., even when the polarization vanishes. The considered pathway is only one possibility out of the many that could occur in an actual material, but is very sound. Indeed, due to the persistence of the AFE distortion throughout, this path involves a quasicontinuous rotation of the electric dipoles associated with individual Bi cations, which are always in an off-centered, low-energy position. We also considered the transformation from $(+P, +A, +\omega)$ to the equivalent state $(-P, -A, +\omega)$ and found that this possibility, which involves the switching of the AFE vector, has a higher-energy barrier of 0.84 eV/f.u. associated with it.

Figure 2 also shows that two solutions $(P, +A, +\omega)$ and $(P, +A, -\omega)$ exist when P ranges from -0.60 to 0.60 C/m^2,

with $(P, +A, +\omega)$ [respectively, $(P, +A, -\omega)$] having a lower energy for positive (respectively, negative) polarization—as is consistent with Eq. (1). On the other hand, only one of these two solutions is found for larger magnitudes of P. Such a result can be understood by Eq. (1) that indicates that the difference in energy between the $(P, +A, +\omega)$ and $(P, +A, -\omega)$ states is $-2C_1 PA\omega$ and thus increases with the magnitude of P. For large values of P, the state with higher energy thus becomes unstable, and only the state with lower energy [that is, $(+P, +A, +\omega)$ for large positive P or $(-P, +A, -\omega)$ for negative P having a large magnitude] can persist. Figure 2(c) further shows that the behavior of the z component of the AFD vector ω as a function of P is quite complex, both when ω is positive or negative. As also shown in Fig. 2(c), such behaviors can be fitted by a polynomial of fourth order in P (that is derived in the Supplemental Material [28]).

Trilinear couplings involving P have also been proposed for the layered $Ca_3Mn_2O_7$ [17], $PbTiO_3/SrTiO_3$ superlattices [31], and strained $CaTiO_3$ [32]. However, the other two quantities appearing in the trilinear couplings of these systems are either two different AFD motions [17,31] or two different antipolar modes [32]. The proposed Eq. (1) is therefore original since three different physical quantities (polarization, AFE, and AFD motions) are intertwined. Moreover, the polarizations involved in the trilinear couplings of Refs. [17,31,32] are small (about 10^{-6} to 0.2 C/m^2), while the polarization of our equilibrium $Pmc2_1$ phase is much larger (namely, 1.12 C/m^2). Moreover, our footnote or Ref. [33] provides a discussion about the nature of this latter polarization (that is, proper versus improper).

Let us now investigate if the polarization-induced switching between $(+P, +A, +\omega)$ and $(-P, +A, -\omega)$ can have some consequence on magnetism. For that, let us first choose a G-type antiferromagnetic (AFM) vector $\mathbf{G}$ being aligned along [110] to demonstrate magnetoelectric switching [35]. Our calculations predict that, in that case, a weak A-type AFM vector (to be denoted by $\mathbf{A}_{\text{AFM}}$) is created along $[\bar{1}10]$ if the system is in the $(+P, +A, +\omega)$ equilibrium state, while it is along the opposite $[1\bar{1}0]$ direction if the system is in the $(-P, +A, -\omega)$ equilibrium state (see Fig. 1) [27]. One should thus be able to reverse the direction of the weak AFM vector $\mathbf{A}_{\text{AFM}}$ when applying an external electric field [since such a field should induce the switching between $(+P, +A, +\omega)$ and $(-P, +A, -\omega)$ states]. To shed more light on such an effect, Fig. 3 shows the evolution of the projection of $\mathbf{A}_{\text{AFM}}$ onto $[1\bar{1}0]$ for the paths considered in Fig. 2, that is, as a function of P varying between $+1.12$ and -1.12 C/m^2. This projection is denoted as A_{AFM}. Continuously decreasing P from its largest studied positive value to its largest-in-magnitude negative value leads to the following behaviors: (i) the negative A_{AFM} first decreases in strength until P is close to $+0.75$ C/m^2; (ii) the negative A_{AFM} then increases in magnitude until exhibiting a maximum for small polarizations; and (iii) the A_{AFM} remains negative and decreases again in magnitude to suddenly jump for a negative P that is in between -0.6 and -0.8 C/m^2 and then adopts a positive
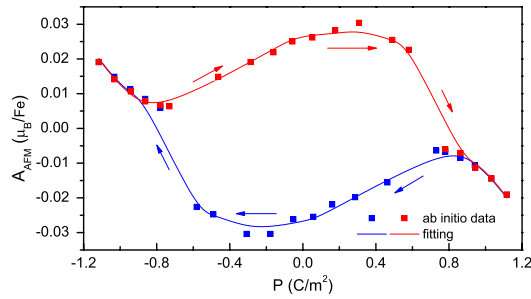
FIG. 3 (color online).   Evolution of the A-type AFM vector A_{AFM} as a function of P. The square symbols show the values predicted from first principles. The solid lines represent the fitting of these data by $A_{AFM} = -0.00051G\omega + 0.059GAP + 0.00011G\omega P^2 - 0.064GAP^3$, where G is the G-type AFM vector (that has a magnitude of around $4\mu_B$), A is the polarization-dependent AFE vector displayed in Fig. 2(b), and ω is the in-phase oxygen octahedral tilting [that also depends on P, as shown in Fig. 2(c)].

value for P less than -0.8 C/m². The change in sign of A_{AFM} occurs precisely when ω also reverts its sign [see Fig. 2(c)] along the equilibrium $(+P, +A, +\omega) \rightarrow$ equilibrium $(-P, +A, -\omega)$ pathway. Figure 3 also shows that A_{AFM} behaves in a mirroring fashion when studying the reverse $(-P, +A, -\omega) \rightarrow (+P, +A, +\omega)$ pathway. Throughout these two pathways, we numerically found that the G-type antiferromagnetic vector not only remains large in magnitude (close to 4 bohr magneton) but also stays oriented along [110]. To understand these effects, one has to recall that Ref. [36] suggested an energy

$$\Delta E_2 = -C_2 \boldsymbol{\omega} \cdot (\mathbf{G} \times \mathbf{A}_{AFM}), \qquad (2)$$

where C_2 is a positive coefficient. In other words, $\boldsymbol{\omega}$, $\mathbf{G}$, and $\mathbf{A}_{AFM}$ want to form a direct triad, as schematized in Fig. 1. Such an equation explains why the combined existence of a G-type AFM vector and in-phase oxygen octahedral tilting results in a weak A-type AFM vector. It also explains why the polarization-induced switching of $\boldsymbol{\omega}$ [such a switch is driven by Eq. (1)] leads to a reversal of $\mathbf{A}_{AFM}$ (see Fig. 1). The control of the $\mathbf{A}_{AFM}$ vector by an electric field is thus made possible via a two-step process [described by Eqs. (1) and (2)], both of which involve AFD motions. Such a two-step process represents a novel magnetoelectric effect. As is also detailed in the Supplemental Material [28], the nontrivial behavior of $\mathbf{A}_{AFM}$ as a function of polarization (Fig. 3) can be reproduced from the energy terms discussed above.

The proposed control of magnetism by polarization is not restricted to the switching of the A-type AFM vector. For instance, let us imagine a $Pmc2_1$ state for which the predominant magnetic ordering is of C-type. Reference [36] tells us that Eq. (2) would have to be replaced by $\Delta E_2 = -C_2 \boldsymbol{\omega} \cdot (\mathbf{C}_{AFM} \times \mathbf{F})$, where $\mathbf{C}_{AFM}$ is the C-type AFM vector and $\mathbf{F}$ is the (weak) ferromagnetic vector. Combining this latter equation with Eq. (1) implies that a net magnetic moment should also be controllable by polarization, in that case. Further simulations we conducted indeed

confirm such an exciting effect. Moreover, the discovered two-step control of the secondary magnetic order parameter is not restricted to BFO, since Eqs. (1) and (2) emerge from symmetry considerations that are not material specific.

[1] M. Fiebig, J. Phys. D **38**, R123 (2005).
[2] Z. J. Huang, Y. Cao, Y. Y. Sun, Y. Y. Xue, and C. W. Chu, Phys. Rev. B **56**, 2623 (1997).
[3] T. Kimura, T. Goto, H. Shintani, K. Ishizaka, T. Arima, and Y. Tokura, Nature (London) **426**, 55 (2003).
[4] T. Lottermoser, T. Lonkai, U. Amann, D. Hohlwein, J. Ihringer, and M. Fiebig, Nature (London) **430**, 541 (2004).
[5] C. Ederer and N. A. Spaldin, Phys. Rev. B **74**, 020401 (2006).
[6] C. Ederer and C. J. Fennie, J. Phys. Condens. Matter **20**, 434219 (2008).
[7] C. J. Fennie, Phys. Rev. Lett. **100**, 167203 (2008).
[8] I. Dzyaloshinsky, J. Phys. Chem. Solids **4**, 241 (1958).
[9] T. Moriya, Phys. Rev. Lett. **4**, 228 (1960).
[10] J. F. Scott and R. Blinc, J. Phys. Condens. Matter **23**, 113202 (2011).
[11] S. Prosandeev, I. A. Kornev, and L. Bellaiche, Phys. Rev. B **83**, 020102(R) (2011).
[12] I. Sosnowska and A. Zvezdin, J. Magn. Magn. Mater. **140–144**, 167 (1995).
[13] M. Mostovoy, Phys. Rev. Lett. **96**, 067601 (2006).
[14] H. Katsura, N. Nagaosa, and A. V. Balatsky, Phys. Rev. Lett. **95**, 057205 (2005).
[15] D. Rahmedov, D. Wang, J. Íñiguez, and L. Bellaiche, Phys. Rev. Lett. **109**, 037207 (2012).
[16] A. Raeliarijaona, S. Singh, H. Fu, and L. Bellaiche, Phys. Rev. Lett. **110**, 137205 (2013).
[17] N. A. Benedek and C. J. Fennie, Phys. Rev. Lett. **106**, 107204 (2011).
[18] G. Kresse and D. Joubert, Phys. Rev. B **59**, 1758 (1999).
[19] S. Prosandeev, I. A. Kornev, and L. Bellaiche, Phys. Rev. Lett. **107**, 117602 (2011).
[20] Y. Yang, W. Ren, M. Stengel, X. H. Yan, and L. Bellaiche, Phys. Rev. Lett. **109**, 057602 (2012).
[21] Y. Yang, M. Stengel, W. Ren, X. H. Yan, and L. Bellaiche, Phys. Rev. B **86**, 144114 (2012).
[22] V. I. Anisimov, F. Aryasetiawan, and A. I. Lichtenstein, J. Phys. Condens. Matter **9**, 767 (1997).
[23] I. A. Kornev, S. Lisenkov, R. Haumont, B. Dkhil, and L. Bellaiche, Phys. Rev. Lett. **99**, 227602 (2007).
[24] Z. Chen, S. Prosandeev, Z. L. Luo, W. Ren, Y. Qi, C. W. Huang, L. You, C. Gao, I. A. Kornew, T. Wu, et al., Phys. Rev. B **84**, 094116 (2011).

[25] R. J. Zeches, M. D. Rossell, J. X. Zhang, A. J. Hatt, Q. He, C.-H. Yang, A. Kumar, C. H. Wang, A. Melville, C. Adamo, *et al.*, Science **326**, 977 (2009).

[26] R. D. King-Smith and D. Vanderbilt, Phys. Rev. B **47**, 1651 (1993).

[27] The AFE vector $\mathbf{A}$ is defined as $\mathbf{A} = 1/N \sum_j d_{\mathrm{Bi},A,j}(-1)^{l_j+m_j}$, where the sum runs over all the N Bi sites j, and where $d_{\mathrm{Bi},A,j}$ is the displacement of the Bi ion at site j that is induced by antiferroelectricity. The site j is located at $a_{\mathrm{lat}}(l_j\mathbf{x} + m_j\mathbf{y} + n_j\mathbf{z})$ from a Bi site chosen as the origin, where a_{lat} is the five-atom cubic lattice constant and where l_j, m_j, and n_j are all integers. Similarly, the in-phase AFD vector ω is defined as $\omega = 1/N \sum_k \omega_k (-1)^{l_k+m_k}$, where the sum runs over all the N Fe sites k, and where ω_k is the vector characterizing the tilting centered on the Fe site k. The latter site is located at $a_{\mathrm{lat}}(l_k\mathbf{x} + m_k\mathbf{y} + n_k\mathbf{z})$ from an Fe site selected as the origin, with l_k, m_k, and n_k being integers. The specific Bi and Fe atoms that have been chosen as the origins to define $\mathbf{A}$ and ω, respectively, are indicated in the middle panels of Fig. 1. Note that the AFM vectors $\mathbf{A}_{\mathrm{AFM}}$ and $\mathbf{G}$ are defined by $\mathbf{A}_{\mathrm{AFM}} = 1/N \sum_k \mu_k (-1)^{n_k}$ and $\mathbf{G} = 1/N \sum_k \mu_k (-1)^{l_k+m_k+n_k}$, where μ_k is the magnetic moment at Fe site k.

[28] See Supplemental Material at http://link.aps.org/supplemental/10.1103/PhysRevLett.112.057202 for additional details and derivations related to the energy of Eq. (1), as well as, to the dependence of the antiferrodistortive vector and (weak) A-type antiferromagnetic vector on polarization.

[29] Note that dividing this barrier of 0.36 eV per formula unit by the spontaneous electric dipole moment (that is, the product between the polarization and the unit volume) of the investigated system in its equilibrium phase yields an electric field of 0.8×10^9 V/m. Such a field has the same order of magnitude as the one recently experimentally applied in BFO films (that is, 10^9 V/m) [30]. This implies that the barrier of 0.36 eV per formula unit can be overcome by a realistic electric field. Moreover, this barrier should decrease when increasing the temperature, rendering the electric field needed to overcome the barrier even smaller and easier to experimentally achieve at finite temperature.

[30] H. Yamada *et al.*, ACS Nano **7**, 5385 (2013).

[31] E. Bousquet, M. Dawber, N. Stucki, C. Lichtensteiger, P. Hermet, S. Gariglio, J.-M. Triscone, and P. Ghosez, Nature (London) **452**, 732 (2008).

[32] Q. Zhou and K. M. Rabe, arXiv:1306.1839v1.

[33] Computing the total energy as a function of polarization, once starting from the $P4/mmm$ phase (which is obtained from the ideal cubic structure by imposing the epitaxial constraint) and setting the AFE and AFD vectors to both vanish, constitutes what we will call "case 1." It leads to a symmetric double well with an energy gain of 0.78 eV per formula unit, with the energy-versus-polarization curve being nicely fitted by a polynomial solely involving the second and fourth powers of the polarization. This is the strongest instability of the reference structure, since letting only the AFE (respectively, AFD) motions occur results in a energy gain of 0.67 eV (respectively, 0.44 eV) per formula unit. As a result, our system can be classified as a "proper ferroelectric" if one uses the $P4/mmm$ phase as a reference. Let us now consider another reference structure, that is, the $Pmc2_1$ state, for which the polarization is zero but for which the AFE and AFD

vectors are optimized to minimize the total energy. Such a new reference structure has four equivalent minima—that are $(+A, +\omega)$, $(-A, +\omega)$, $(+A, -\omega)$, and $(-A, -\omega)$—with an energy gain of 0.92 eV per formula unit with respect to the $P4/mmm$ phase that is larger than the instability due to polarization only. Moreover, starting from the $(+A, +\omega)$ minimum and allowing the polarization to vary from negative to positive values (while freezing the A and ω values) constitutes what we call "case 2" in the following. It leads to an energy-versus-polarization single well having an energy gain of 1.05 eV per formula unit with respect to the $P4/mmm$ phase, with the energy being nearly linear around $P = 0$ [as is consistent with the trilinear coupling of Eq. (1)]. Fitting this energy-versus-polarization curve by a polynomial up to fourth order in polarization yields a negative linear coefficient [as is also consistent with the trilinear coupling of Eq. (1)], while the quadratic parameter is still negative but has a magnitude around 19 times smaller than that in case 1. Let us finally consider another $Pmc2_1$ structure as a reference that is the one for which the polarization still vanishes but the AFE and AFD vectors are those of the equilibrium $Pmc2_1$ state (for which P, A, and ω are all optimized to minimize the total energy). This second $Pmc2_1$ reference structure also has four equivalent minima (due to the possible positive and negative signs of A and ω) with an energy gain of 0.76 eV per formula unit with respect to the $P4/mmm$ phase that is now slightly smaller than the instability due to polarization only. Starting from the $(+A, +\omega)$ minima and letting the polarization vary from negative to positive values (while freezing the A and ω values) constitutes what we we denote as "case 3." It results in an energy-versus-polarization curve that is still nearly linear around $P = 0$, but such a curve now has a double well that is asymmetric (the lowest well has an energy gain of 1.29 eV per formula unit with respect to the $P4/mmm$ phase). Such a change in shape of the energy-versus-polarization curve with respect to case 2 arises from the fact that its fitting by a polynomial up to fourth order in polarization still yields a negative linear coefficient as in case 2, but the magnitude of the negative quadratic parameter is now about 6 times larger than that in case 2. This dramatic change of the magnitude of the quadratic term between case 1, case 2, and case 3 originates from the sum between the (negative) b' coefficient and the (positive) $e\omega^2 + fA^2$ terms introduced in Eq. (8) of the Supplemental Material [28], since these latter terms depend on the magnitude of the AFD and AFE vectors (note that case 3 has a much lower ω than case 2 due to the biquadratic repulsion between AFD motions and polarization). All the results indicated here may imply that the traditional concept of proper-versus-improper ferroelectricity can be rather subtle in our case and may have to be revisited or generalized [34]. They also suggest that, in systems like this one, it may be mandatory to study temperature-dependent properties in order to determine the character of the ferroelectricity.

[34] M. Stengel, C. J. Fennie, and P. Ghosez, Phys. Rev. B **86**, 094112 (2012).

[35] Additional first-principles calculations indicate that the total energy is quasidegenerate (namely, within 0.7 meV/5 atoms) when placing $\mathbf{G}$ along several high-symmetry directions, with a minute preference for the G-type AFM vector to lie along [001].

[36] L. Bellaiche, Z. Gui, and I. A. Kornev, J. Phys. Condens. Matter **24**, 312201 (2012).